Enhanced stability of electrochemical performance of few-layer black phosphorus electrodes by noncovalent adsorption of 1,4-diamine-9,10-anthraquinone

Paweł Jakóbczyk[1]*, Anna Dettlaff[2], Grzegorz Skowierzak[3], Tadeusz Ossowski[3], Jacek Ryl[4], Robert Bogdanowicz[1]

[1]Department of Metrology and Optoelectronics, Faculty of Electronics, Telecommunications and Informatics, Gdańsk University of Technology, Gabriela Narutowicza 11/12, 80-233 Gdańsk, Poland
[2] Department of Energy Conversion and Storage, Faculty of Chemistry, Gdańsk University of Technology, Gabriela Narutowicza 11/12, 80-233 Gdańsk, Poland
[3] Department of Analytical Chemistry, Faculty of Chemistry, University of Gdańsk, 63 Wita Stwosza St., 80-952 Gdańsk, Poland
[4] Institute of Nanotechnology and Materials Engineering, Faculty of Applied Physics and Mathematics, Gdańsk University of Technology, Gabriela Narutowicza 11/12, 80-233 Gdańsk, Poland

* Corresponding author.

E-mail address: pawel.jakobczyk@pg.edu.pl (P. Jakóbczyk).

Abstract

In this paper, the novel noncovalent functionalisation strategy of few-layer black phosphorus by 1,4-diamine-9,10-anthraquinone electrode was proposed and studied. The degradation of few-layer black phosphorus under exposure to oxygen and water is a significant obstacle to its use as an electroanalytical electrode. The anthraquinone compound adsorbed at black phosphorus flakes results in improved prevention of the phosphorus surface against degradation and electrode decomposition. Furthermore, a large concentration of amino group present in 1,4-diamine-9,10-anthraquinone enhances the electrochemical performance of electrode revealed by a faster rate of heterogeneous electron transfer observed in cyclic voltammetry studies. The designed electrode exhibits stable redox peaks over 100 cycles with separation between the peaks of 79 ± 2 mV and the formal redox potential reaching 257 ± 3 mV. The differential pulse voltammetry was utilised for the detection of ascorbic acid, revealing a limit of detection equal to 3.29 ppm (18.68 µM) and a limit of quantification of 9.98 ppm (56.66 µM). The linear range of 1-20 ppm was achieved, allowing for the detection of ascorbic acid in real conditions. Thus,

anthraquinone-modified few-layer black phosphorus may be an attractive novel electrode material for sensitive electroanalytical applications.

Keywords: few-layer black phosphorus, 1,4-diamine-9,10-anthraquinone, noncovalent functionalisation, electrochemical properties, electrochemical sensor

1. Introduction

During the last decade, 2D nanomaterials such as transition metal dichalcogenides or graphene have been explored extensively as promising materials for future electronics applications. In 2014, the family of 2D materials was expanded by a new member, phosphorene, a monolayer of black phosphorus - BP (phosphorus allotrope). The phosphorene forms a puckered honeycomb structure in which each phosphorus atom is covalently bonded to 3 nearest neighbours. Similar to graphene and graphite, the BP monolayers are interconnected in black phosphorus by van der Waals interactions. Hence, the bulk black phosphorus can be exfoliated down to a single or few layers using chemical or psychical forces. Recently, the BP nanosheets can be fabricated via electrochemical exfoliation [1,2], ball-milling [3], chemical vapour deposition [4] or ultrasonic liquid phase exfoliation [5–7].

Only a few papers describe the electrochemical properties of phosphorus. Hermes & Scholz described the electrochemical properties of white phosphorus [8]. The electrochemical oxidation layered black phosphorus in different pH has been studied [9]. Dettlaff et al.[7] investigated electrochemical stability of few-layer black phosphorene fabricated in different ultrasonic horn power using voltammetry and impedance technique. Properties of phosphorene like a large surface make it suitable for sensors and catalysis. In order to obtain the required electrochemical properties and stability under ambient conditions, it is subjected to various modifications [10]. BP exhibits anisotropic electrochemical properties, thanks to which the electron transfer is much faster at the edge sites than at the base plane [9]. This strategy was used to build electrochemical sensors. Faster charge transfer [11], higher adsorption [12],

improved conductivity [13,14], protection against degradation [15], defects [16] are the directions of changes in the properties of phosphorene that can be observed in the literature.

Research on phosphorene-based sensors has included: electrochemical sensors [14,17], electrochemical biosensors (enzyme electrodes [18,19], electrochemical aptasensors [20], electrochemical immunosensors [21,22], mixed aptamer immunosensors [23]), electrochemiluminescence [24,25].

The major hurdle for phosphorene in processing and application as the sensor is its fast oxidation and degradation in ambient conditions. Simultaneous dispositions of light, oxygen, and water cause the ageing process [7,26–28]. In order to enhance the ambient stability of phosphorene, its surface can be chemically modified. In particular, the phosphorene has been covalently functionalised by diazonium salt [29], azide [30], nucleophilic reagents [31], and noncovalently by poly-L-lysine [18], anthraquinone [32], and surface encapsulation [33].

Up to date, only Gusmão et al. [32] reported profitable phosphorene modification by anthraquinone for electrochemical application. Nevertheless, they applied plain anthraquinone targeting the application of that system to energy storage applications.

Rapid and cheap determination of vitamin C is still an area researched by scientists due to the great importance of ascorbic acid both for human life (in clinical samples) and applications in the pharmaceutical and food industries. Electrochemical techniques [34–36], spectrophotometry [37], spectrofluorometry [38], fluorescence [39,40], titration [41,42], electrophoresis [43] and high performance liquid chromatography (HPLC) [44,45] are common techniques used to detect ascorbic acid. The electrochemical sensors are the most commonly used by scientists to detect ascorbic acid due to its high sensitivity, low cost and simplicity [46]. A compound with a detection potential below the oxidation potential of phosphorus (0.65 V) [9] was selected for sensory experiment. Ascorbic acid meets this criterion. The detection of

any compound in the phosphorus oxidation potential could lead to an erroneous current response due to phosphorus oxidation.

This work has shown for the first time the noncovalent functionalisation of phosphorene with 1,4-diamine-9,10-anthraquinone (1,4-DAAQ). Applied 1,4-DAAQ has amino moieties resulting in synergistic enhancement of electrochemical properties and delivering surface functional amino groups for further bio-oriented, electroanalytical applications (i.e. antigen or aptamer grafting). 1,4-DAAQ is adsorbed at few-layer black phosphorus (FLBP) and thus protects the phosphorus from rapid degradation under oxygen and water conditions resulting in enhanced stability of the designed electrode. The proposed modified FLBP was successfully used for ascorbic acid detection using differential pulse voltammetry (DPV).

2. Experimental

2.1 Reagents

Black phosphorus (BP, >99.99%) was obtained from Smart Elements. 1-Methyl-2-pyrrolidinone (NMP), anhydrous, purity: 99.5%) was collected from Sigma Aldrich. 1,4-diamino-9,10-anthraquinone (1,4-DAAQ, >90%) was purchased from Fluka. Methanol (MeOH, 99%) was collected from Stanlab. The sodium sulfate (ACS reagent, purity ≥99%, Aldrich), potassium hexacyanoferrate (III) (pure p. a., Chempur), and hydrochloric acid (35-38%, Chempur) aqueous solutions were prepared using demineralised water. The argon was collected from Air Liquid and was of the highest purity class. All reagents were used without further purification.

2.2 Black Phosphorus Liquid Exfoliation and Functionalisation

Pre-crushed BP (30 mg) was added to deoxygenated NMP solvent (7 ml). The process of liquid exfoliation was realised in an ice-cooled bath, at a temperature from 0 to 3 °C, under a stream

of argon using a horn probe ultrasonicator (Bandelin Sonopuls HD2200, 20 kHz). The sonication tip was set to a power of 40 W, and ON/OFF time equals 0.5/0.5 s. The mixture was sonicated in the ice bath (0-3°C) under a stream of argon. The sonication-aided exfoliation process took 4 hours. Afterwards, the resultant suspension was centrifuged at 11 000 rpm for 15 min to remove the residual unexfoliated particles, yielding yellowish supernatant. The few-layer black phosphorus electrode (FLBP electrode) was made by applying the supernatant to a glassy carbon electrode and dried in a vacuum chamber at 60 Celsius degrees. Then the FLBP electrode was immersed in a 0.001 M 1,4-DAAQ solution in methanol: water mixture (volume ratio, 1:1) for 2 h.

The next step was to wash the electrode with a solution of methanol and water (volume ratio, 1: 1). The functionalised FLBP electrode with 1,4-DAAQ (FLBP_1,4-DAAQ electrode) was used for electrochemical measurements. In Fig. 1, the scheme of FLBP noncovalent functionalisation using 1,4-DAAQ is shown.

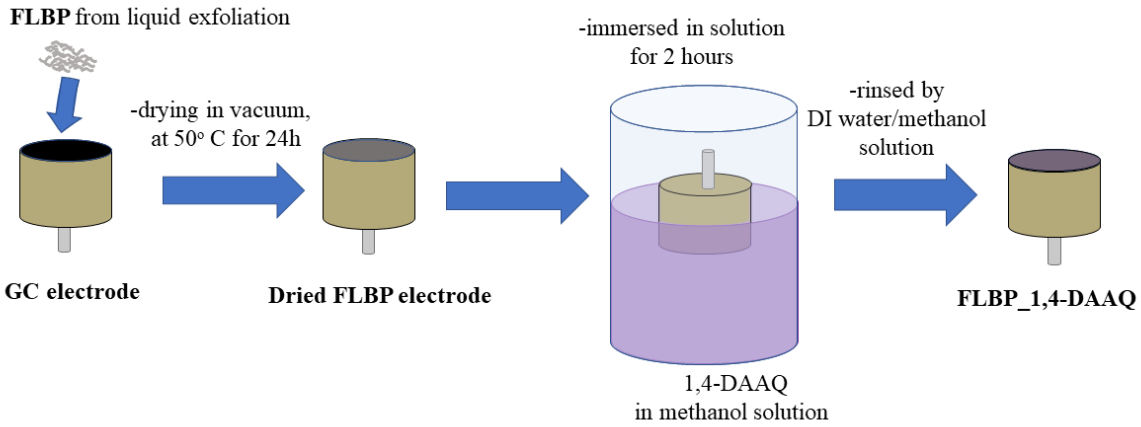

Fig. 1. Scheme of the glassy carbon modification by few-layer black phosphorus and next noncovalent FLBP functionalisation using 1,4-diamino-9,10-anthraquinone.

2.3. Electrode characterisation

X-ray photoelectron spectroscopy (XPS) analysis was carried out to determine changes in the chemical composition of functionalised FLBP electrodes and get information on the oxidation

of FLBP_1,4-DAAQ and FLBP electrode surfaces. XPS measurements were performed using Escalab 250Xi spectroscope (ThermoFisher Scientific) using monochromatic Al Kα X-ray source with a spot diameter of 200 μm and pass energy 20 eV for high-resolution spectra. The adventitious carbon C1s peak at 284.6 eV was used for peak calibration.

The morphology and distribution of FLBP on the surface were characterised by scanning electron microscopy (SEM) and energy-dispersive X-ray (EDX) spectroscopy (Phenom XL instrument, Thermo Fisher Scientific). An accelerating voltage of 15 kV was used with a secondary electron detector (SED) working in high vacuum mode. The electrochemical studies were investigated by cyclic voltammetry (CV) and differential pulse voltammetry (DPV) in the three-electrode system using a potentiostat-galvanostat (VMP-300, BioLogic, France). The working electrode had a working area of 0.071 cm^2, the counter electrode was a platinum wire, and the reference electrode was an AgCl-coated Ag wire in 3M KCl. CV measurements were carried out in 1 M HCl and in 0.5 M Na_2SO_4 5mM $K_3[Fe(CN)_6]$, at a scan rate of 100 mV s^{-1} for potential window and from 10 mV s^{-1} to 700 mV s^{-1} for redox probe tests. The optimisation of DPV parameters such as a pulse height, a pulse width, and scan rate was performed. The parameters influence on the peak current of ascorbic acid during DPV. The highest current of ascorbic acid was for potential height equals 60 mV and was considered as an optimum. However, the pulse width had no visible effect on the increase of the ascorbic acid peak current, therefore the value for which the peak shape was optimal was selected (70 ms). Next, the effect of the scan rate value, ranging from 2 to 50 mV s^{-1} was analyzed. The highest ascorbic peak current was found at the 5 mV s^{-1} scan rate value of 60 mV pulse height and 70 pulse width, so this value was used for subsequent studies. Moreover, the DPV measurements were performed in 0.1 M Na_2SO_4 containing ascorbic acid with 1-20 ppm concentration.

3. Results and discussion

3.1 Surface analysis of functionalised FLBP electrode

The layer of phosphorus particles on the glassy carbon electrode was confirmed by SEM and EDX images (Fig. 2). The deposited phosphorus layer is consisted from nano-size particles, below the resolution of SEM microscope, with a few agglomerates and residues of larger phosphorus particles, ranging in size from several to several dozen micrometres. The surface of the FLPB modified GC electrode (Fig. 2 a,c) and the modified GC electrode by FLBP and then functionalised by 1,4-DAAQ (Fig. 2 b,d) have a similar degree of coverage by phosphorus. The EDX images show that the FLBP, when functionalized by immersion in methanol: water (v / v, 1: 1), does not detach from the glassy carbon surface due to functionalisation, but forms a structurally similar GC cover layer (FLBP_1,4-DAAQ) to FLBP.

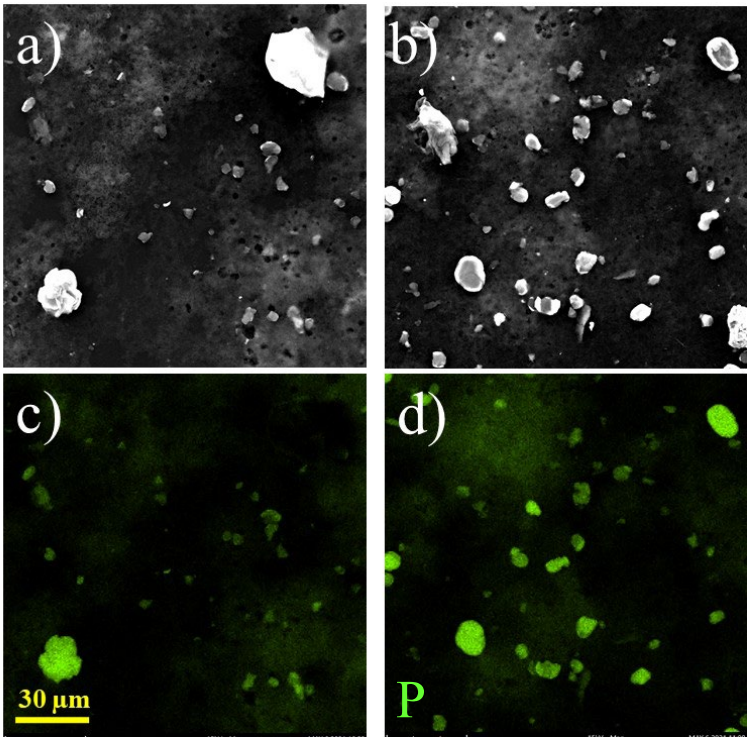

Fig. 2. SEM micro-images of electrode surfaces: (a) FLBP, (b) FLBP_1,4-DAAQ, (c,d) EDX mapping of phosphorus.

The XPS spectra recorded in the core-level binding energy range of the P 2p signal allow us to assess the oxidation state of phosphorous. It can be seen in Figures 3a and 3b that spectra for both FLBP and FLBP_1,4-DAAQ have well-defined P 2p doublets, with the primary P $2p_{3/2}$ component located at 129.8 eV and P $2p_{1/2}$ shifted by +0.5 eV, and ascribed to the P-P bonds. Furthermore, the broad signal occurring ca. 134.1 eV usually is associated with phosphates or phosphorous hydroxides, in line with our previous work and other literature sources [21,22]. This is typical of black phosphorus, which easily oxidises under atmospheric conditions. Notably, the peak intensity decreases significantly in the case of the FLBP_1,4-DAAQ sample (Fig. 3b), suggesting that it is less prone to spontaneous surface oxidation. This negligible oxidation is caused by noncovalent interactions, mainly due to van der Waals forces. It was already noted in the literature that the noncovalent interaction significantly stabilises BP and prevents its oxidation and degradation [32,47]. Finally, the FLBP_1,4-DAAQ sample XPS spectra in the N 1s peak binding energy range (Fig. 3c) may be deconvoluted using two peaks at 398.2 and 400.5 eV and characteristic of C-NH_2 and C-N bonds, respectively [48]. The first of the two is dominant in the recorded spectra, testifying the successful functionalisation of FLBP using 1,4-diamine-9,10-anthraquinone.

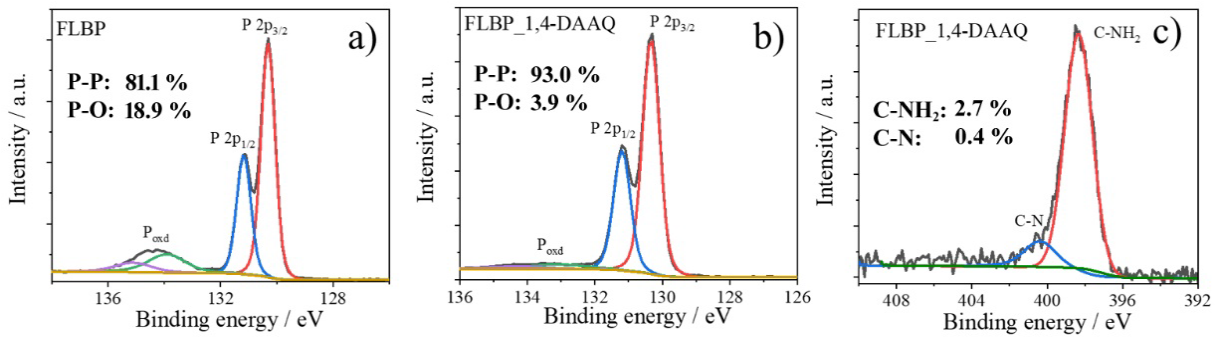

Fig. 3. High-resolution XPS of the P 2p core level for (a) FLBP, and (b) FLBP_1,4-DAAQ. N 1s XPS spectrum of the FLBP_1,4-DAAQ (c).

3.2 Electrochemical properties of FLBP and FLBP_1,4-DAAQ

Functionalisation of the few-layer black phosphorus resulted not only in protection against oxidation but also change the electrochemical properties. Figure 4a shows the cyclic voltammetric behaviour of glassy carbon electrode (GC), modified glassy carbon electrode by few-layer black phosphorus (FLBP), and functionalised FLBP (FLBP_1,4-DAAQ) in acid media (1 M HCl). During cyclic voltammetry (Figure 4a) the oxidation of the pristine FLBP [7,9] and FLBP_1,4-DAAQ at 0.65 V is observed. The oxidation peak of phosphorus for FLBP_1,4-DAAQ is visible but lower than for the pristine phosphorene, which may be due to partial coverage by 1,4-diamine-9,10-anthraquinone and a smaller oxidisable surface. In the following cycles, the peak from FLBP oxidation decreases. Peaks from 1,4-diamine-9,10-anthraquinone shown on the CV curve are attributed to the well-known 2 protons, 2 electrons quinone redox interconversion in acid media [32]. The presence of these peaks confirms the presence of anthraquinone derivatives on the surface of FLBP.

In the next step, fabricated electrodes were investigated versus the ferricyanide/ferrocyanide redox system to investigate the electron transfer behaviour (Figure 4b). Before the functionalisation process of FLBP electrode, one can notice the influence of the partially oxidized surface of the phosphorene on worse charge transfer resulting in a higher peak separation value (ΔE_p=167 ± 8 mV) compared to the ΔE_p equal to 132 ± 4 mV for GC and the lowest ΔE_p after functionalization of FLBP (ΔE_p=80±3 mV). Thanks to noncovalent modification of the FLBP, the electrode exhibited enhanced electrochemical properties (Figure 4b). The surface analysis made with XPS presents that the FLBP has a higher proportion of oxygen than FLBP_1,4-DAAQ (Fig. 3a). The differences in electrochemical properties are influenced by surface termination. Studies on the impact of boron-doped diamond (BDD)

termination by Granger and Swain [49] on the $[Fe(CN)_6]^{3-/4-}$ redox couple reaction show that after surface oxidation of BDD electrode the peak to peak potential separation increases for the ferricyanide/ferrocyanide reaction. After the hydrogen plasma treatment of BDD and the termination change to hydrogen, ΔE returns to the original value and shows the effect of termination on ΔE values. The oxygen causes deterioration of kinetic parameters. In this study, the absence of PO_x groups at the surface of FLBP_1,4-DAAQ as proven by XPS (Fig. 3b), cause decrease of ΔE_p. The presence of $-NH_2$ groups derived from 1,4-DAAQ, which was confirmed electrochemically (Fig. 4b), promote charge transfer between the solution of $K_3[Fe(CN)_6]$ and the functionalised electrode [11,50]. No deterioration can be seen in the course of subsequent cycles (Fig. 4c), so there is also no formation of irreversible adsorbates of $[Fe(CN)_6]^{3-/4-}$ as it occurs at the platinum surface [49].

From the CV curves recorded in redox system it is also feasible to determine the electrode reaction kinetics [51]. Hence, it is possible to measure the reaction of electron transfer through the modified and unmodified FLBP electrodes. The estimated electrochemical parameters are gathered in Table 1. As can be seen, higher peak current densities of oxidation ($j_{p,ox}$) and reduction ($j_{p,red}$) of redox mediator are promoted on the FLBP_1,4-DAAQ electrode. The values of $j_{p,ox}$ are equal to 0.88 ± 0.03 mA cm^{-2} and 0.57 mA cm^{-2} for FLBP_1,4-DAAQ and FLBP, respectively, which follows from lower electrode resistance and easier charge transfer which can also be related to the presence of 1,4-diamine-9,10-anthraquinone on the electrode surface [11].

The heterogeneous electron transfer k^o for FLBP and FLBP_1,4-DAAQ were calculated using Eq. (1) according to the Nicholson method [52,53].

$$k^\circ = \psi \cdot \sqrt{\frac{\pi \cdot D \cdot \nu \cdot F \cdot n}{R \cdot T}} \qquad (1)$$

where ψ is a kinetic parameter, D corresponds to the diffusion coefficient ($7.6 \cdot 10^{-6}$ cm^2 s^{-1}) [54,55], ν is the scan rate, n reflects the number of electrons, R is the molar gas constant, T is the temperature.

Table 1. Comparison of electrochemical parameters of FLBP-based electrode estimated for 100 mV s^{-1} scan rate.

	FLBP_1,4-DAAQ	**FLBP**
$E_{p,ox}$ / **mV**	297± 5	332± 7
$j_{p,ox}$ / **mA cm^{-2}**	0.88 ± 0.03	0.57± 0.07
$E_{p,red}$ / **mV**	217± 4	165± 6
$j_{p,red}$ / **mA cm^{-2}**	0.93± 0.04	0.63± 0.06
$j_{p,red}$ / $j_{p,ox}$	1.06	1.11
ΔE_p / **mV**	80± 3	167± 8
E_f / **mV**	257 ± 6	249±9
Λ	2.36	0.35
Ψ	1.33	0.20
k^o / **cm s^{-1}**	$1.29 \cdot 10^{-2}$	$1.88 \cdot 10^{-3}$

*assumption: charge transfer coefficient α = 0.5

FLBP_1,4-DAAQ shows a faster rate of heterogeneous electron transfer compared to the layer without functionalisation ($1.29 \cdot 10^{-2}$ cm s^{-1} and $1.88 \cdot 10^{-3}$ cm s^{-1}, respectively), which indicates better electron transfer of the layer than the bare FLBP.

Furthermore, the value of the half potential, $E_{p/2}$, for electrochemically reversible reaction should be equal to 56.5 mV and the $j_{p,red}$ / $j_{p,ox}$ ratio is 1 [54]. In our case, for the FLBP_1,4-DAAQ electrode the values are slightly higher $E_{p/2}$ = 58 mV and $j_{p,red}$ / $j_{p,ox}$ = 1.06, which suggest a electrochemically quasi-reversible nature of electrode process. In order to confirm the quasi-reversible reaction the Matsuda and Ayabe Λ parameter was calculated using Eq. (2) [54,56].

$$\Lambda = k^{\circ} \cdot \sqrt{\frac{R \cdot T}{F \cdot D \cdot \nu \cdot n}} \qquad (2)$$

The estimated Λ values are equal to 0.35 and 2.36 for FLBP and FLBP_1,4-DAAQ, respectively. For both electrodes, the value of Matsuda and Ayabe parameter is in the quasi-reversible zone ($15 > \Lambda > 10^{-3}$) [56], which indicate quasi-reversible redox reactions of $[Fe(CN)_6]^{3-/4-}$ pair for scan rate of 100 mV s^{-1}. Thus, both mass transport and charge transfer influence the electrode reaction [54,56,57]. However, the parameters calculated for functionalised electrode show more facile electrode kinetics and are closer to the values corresponding to reversible reactions. Other parameters also suggest a quasi-reversible reaction. The kinetic parameter ψ for FLBP it is much lower and amounts to only 0.2 (ψ = 0.001 refers to a totally irreversible reaction [52]). The previously calculated HET is also in a region classified as quasi-reversible, i.e. in the range from 0.095 cm s^{-1} to $6.32 \cdot 10^{-6}$ cm s^{-1} (T = 298 K, $\nu = 0.1$ V s^{-1}, $D = 7.6 \cdot 10^{-6}$ cm^2 s^{-1}, and $\alpha = 0.5$) [54,56].

Characterisation of electrochemical processes in terms of electrode stability was performed by 100 cycles (Figure 4c) in the ferricyanide/ferrocyanide redox system in a basic electrolyte solution (0.5 M Na_2SO_4) below the phosphorus oxidation potential. The $[Fe(CN)_6]^{3-/4-}$ has a similar interaction with the surface as ascorbic acid [49,50], in both cases there is outer sphere electron transfer, therefore the stability of the system is shown for the $[Fe(CN)_6]^{3-/4-}$ redox system. Current response after 100 cycles slightly increased (7.4%). The separation between the peaks (ΔE_p) after 100 cycles is stable at 79 ± 2 mV, while the formal redox potential (E_f) was 257 ± 3 mV. The stability of the electrode operation can also be observed after the slight variation of the peak currents after the initial cycle. The ideal reversible electrochemical behaviour demonstrates the strong adsorption of 1,4-DAAQ on the electrode surface.

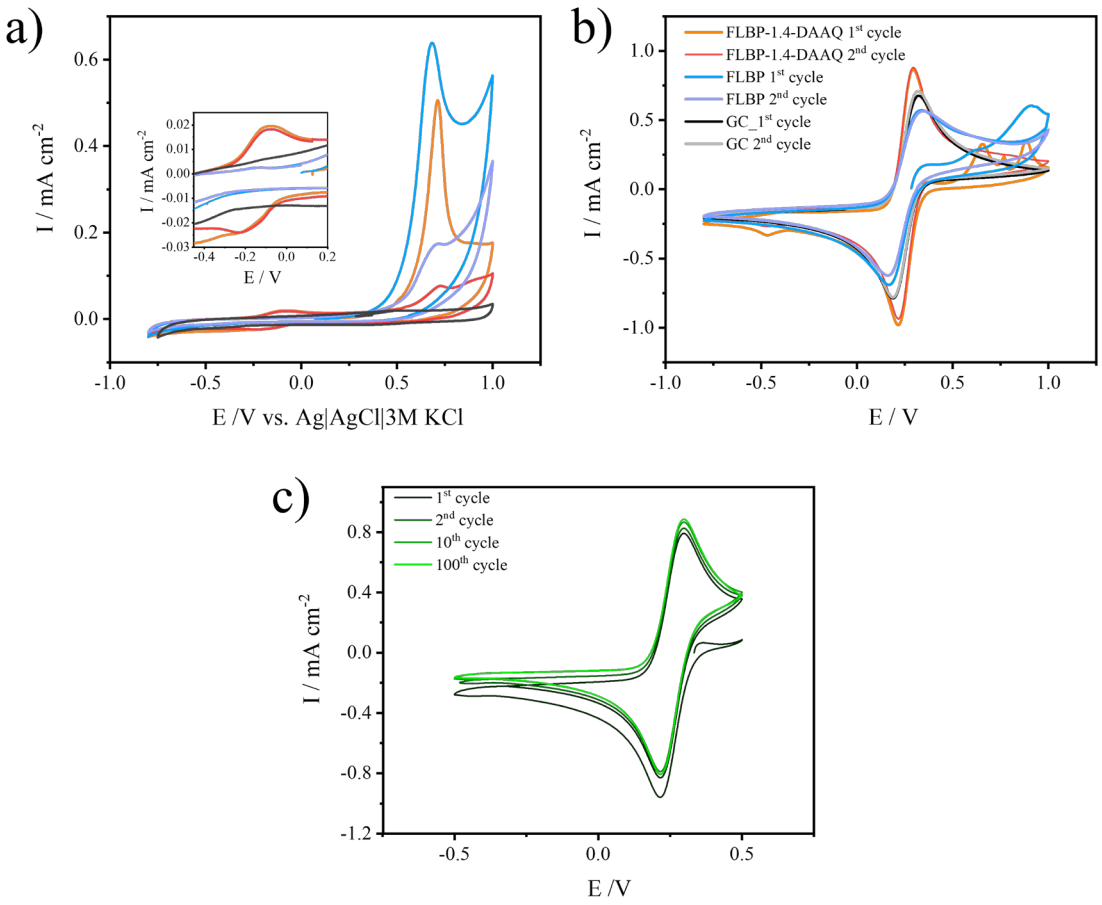

Fig. 4. CVs obtained for a) GC, FLBP, FLBP_1,4-DAAQ electrode in 1M HCl; b) GC, FLBP, FLBP_1,4-DAAQ electrode in 1 mM $K_3[Fe(CN)_6]$ in 0.5 Na_2SO_4; c) FLBP_1,4-DAAQ electrode in 1 mM $K_3[Fe(CN)_6]$ in 0.5 Na_2SO_4; vs. Ag/AgCl in 3M KCl. Scan rate: 100 mV s^{-1}.

On the basis of the shape of the voltammograms, the limiting factor of the process could be predicted. The bell-type shape of curves corresponds to an adsorption wave or a draw-out type corresponding to a diffusional-type wave. Figure 5a displays the draw-out waves, but their shape is strongly affected by chemical interactions with reaction intermediates and solvent molecules, e.g., partially surface oxidised phosphorene and residuals of NMP from FLBP fabrication step, 1,4-DAAQ adsorption. When redox species in solution are partially adsorbed to the surface, the electrode process is far from predictable shape typical for adsorption due to the very high concentration in the adsorbed state. However, according to the literature, a draw-out-shaped wave also could be observed for the adsorbed control reaction [58]. Deviations of the curves may be attributed to electrostatic effects incurred by neighbouring charged species

[59]. The capacitive nature of the current response complicates the determination of ongoing processes. The curve's character could interfere with the diffusion process. Due to the mentioned elements, it is challenging to determine the nature of the processes taking place on the electrode. However, the curve shows the dependence characteristic for diffusion (linear dependence of the peak currents on the square root of the scan rate) (Fig. 5b). As can be seen, the cathodic and anodic peak currents increased with the sweep rate. Moreover, there is an asymmetry between the oxidation and reduction peaks, which demonstrated a more complex electrode process related as previously mentioned interactions with NMP residuals.

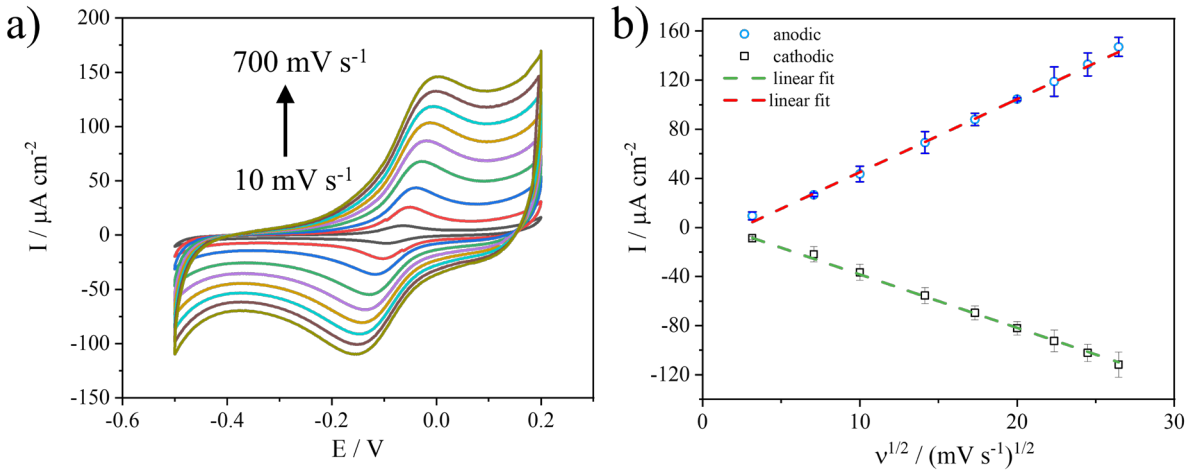

Fig. 5. Cyclic voltammograms of a) FLBP_1,4-DAAQ electrode in 1M HCl at scan rates from 10 to 700 mV s^{-1}. The linear variation of the Faradaic process of b) FLBP_1,4-DAAQ electrode, the dependence of the peak current of the electrode process on the square root of the scan rate.

3.3 Detection of ascorbic acid on the FLBP_1,4-DAAQ electrode

The functionalised electrode (FLBP_1,4-DAAQ) was used to determine ascorbic acid in 0.1 M Na_2SO_4 solution. Differential pulse voltammetry (DPV) was applied as the detection method due to excellent background suppression and higher sensitivity than the CV technique. The FLBP_1,4-DAAQ electrode, thanks to the use of 1,4-diamine-9,10-anthraquinone enhancing electroanalytical properties, could be utilised for electrochemical detection.

Figure 6a exhibits the current response versus increasing ascorbic acid concentrations in the range from 1 to 20 ppm. Figure 6b shows a linear calibration curve (R^2=0.998) over the 1-20 ppm concentration range. The resulting linear dependence is characterised by a high value of the slope coefficient (0.572 µA cm^{-2} ppm^{-1}), which proves the high sensitivity of the tested electrode. The adsorbed 1,4-diamine-9,10-anthraquinone molecules are ascribed for improved detection since they attract ascorbic acid molecules by the π-π interactions. Additionally, the -NH_2 groups of the adsorbed compound enhance the electron transfer in the electrode reaction.

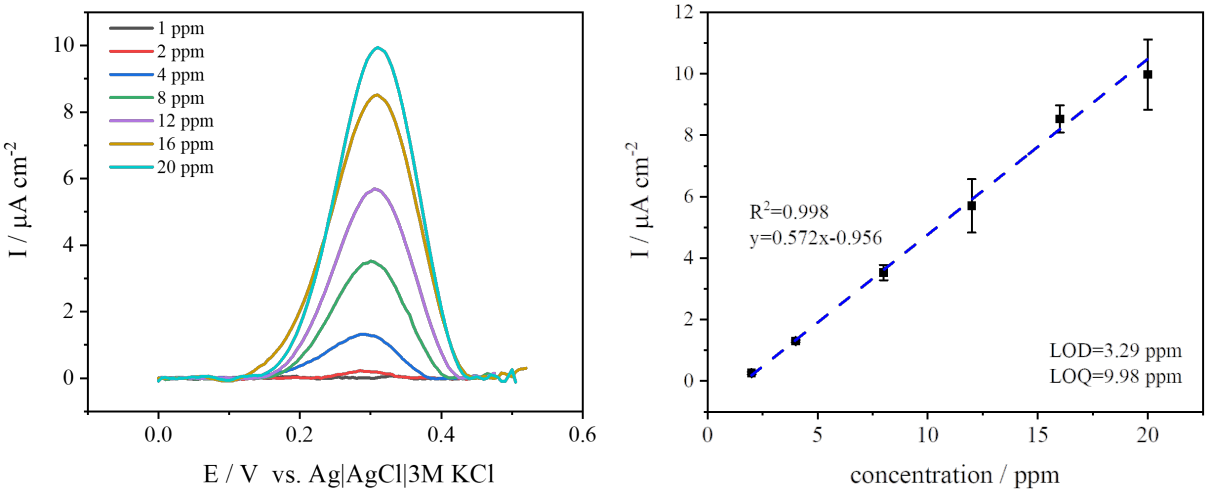

Fig. 6. Detection of ascorbic acid: a) Differential pulse voltammograms of varying ascorbic acid concentrations in 0.1 M Na_2SO_4 in the range from 1 ppm to 20.0 ppm; b) the linear fit of concentration vs peak current density of FLBP_1,4-DAAQ electrode.

To investigate the electrode-to-electrode reproducibility, five different electrodes were used to determine 12 ppm ascorbic acid. The current responses for this electrochemical sensor offered the reproducible responses with a 1.51% relative standard deviation (RSD), demonstrating good reproducibility. The limit of detection (LOD) and the limit of quantification (LOQ) were calculated using the method based on the equations containing the standard deviation (σ) of the estimated value (net signal), as is the slope of the calibration curve (s): LOD = 3.3 σ / s, LOQ = 10 σ / s [60]. The limit of detection was 3.29 ppm (18.68 µM), and the LOQ was 9.98 ppm (56.66 µM) ascorbic acid. The linear range of 1-20 ppm was achieved, allowing for the

detection of ascorbic acid in real conditions. In this work, better values of sensitivity (0.572 μA cm^{-2} ppm^{-1}) were obtained than Zhang et al., who modified glassy carbon electrodes using the poly(acid chrome blue K). Also, the limit of detection obtained with the FLBP_1,4-DAAQ electrode is better than, e.g., polyaniline modified screen-printed carbon electrode [61]. There are also known electrodes with a lower LOD (0.05 μM) in the literature, but they have a lower linear range and are expensive, e.g., gold nanoparticles modified electrode [62]. FLBP_1,4-DAAQ electrode has properties that allow satisfactory detection of ascorbic acid over a wide range of concentrations.

Conclusions

The degradation of phosphorus under exposition conditions to oxygen and water is a significant obstacle to its use as sensors. The proposed functionalisation in this work with 1,4-diamine-9,10-anthraquinone enhanced the stability in ambient conditions of FLBP while improving charge transfer in redox reactions. Noncovalent functionalised FLBP electrodes show that 1,4-diamine-9,10-anthraquinone is anchored to FLBP and exhibits redox peaks that are stable over 100 cycles. Moreover, the fabricated FLBP_1,4-DAAQ electrode was used for the detection of ascorbic acid.

The developed electrochemical sensor combines a low detection limit with significant sensitivities and a wide linear concentration range for ascorbic acid detection. Other electrodes tend to have one of these advantages and become less useful. Thus, FLBP_1,4-DAAQ may be an attractive novel electrode material for the sensitive detection of ascorbic acid.

Declaration of Competing Interest

The authors declare that there are no competing financial interests or personal relationships that could have appeared to influence the work reported in this paper.

Credit authorship contribution statement

Paweł Jakóbczyk: Conceptualisation, Formal analysis, Investigation, Writing – original draft, Writing – review & editing. **Anna Dettlaff:** Writing – review & editing. **Jacek Ryl:** Formal analysis, Writing review & editing. **Grzegorz Skowierzak:** Investigation**. Tadeusz Ossowski,** review & editing**. Robert Bogdanowicz:** Writing – review & editing, Funding acquisition.

Acknowledgements

This work was supported by the Polish National Science Centre [2016/22/E/ST7/00102].

References

[1] A. Ambrosi, Z. Sofer, M. Pumera, Electrochemical Exfoliation of Layered Black Phosphorus into Phosphorene, Angew. Chemie - Int. Ed. (2017). doi:10.1002/anie.201705071.

[2] H. Xiao, M. Zhao, J. Zhang, X. Ma, J. Zhang, T. Hu, T. Tang, J. Jia, H. Wu, Electrochemical cathode exfoliation of bulky black phosphorus into few-layer phosphorene nanosheets, Electrochem. Commun. (2018). doi:10.1016/j.elecom.2018.02.010.

[3] L. Shao, H. Sun, L. Miao, X. Chen, M. Han, J. Sun, S. Liu, L. Li, F. Cheng, J. Chen, Facile preparation of NH2 -functionalized black phosphorene for the electrocatalytic hydrogen evolution reaction, J. Mater. Chem. A. 6 (2018) 2494–2499. doi:10.1039/C7TA10884B.

[4] J.B. Smith, D. Hagaman, H.F. Ji, Growth of 2D black phosphorus film from chemical vapor deposition, Nanotechnology. 27 (2016) 1–8. doi:10.1088/0957-4484/27/21/215602.

[5] Y. Zhang, N. Dong, H. Tao, C. Yan, J. Huang, T. Liu, A.W. Robertson, J. Texter, J. Wang, Z. Sun, Exfoliation of Stable 2D Black Phosphorus for Device Fabrication, Chem. Mater. 29 (2017) 6445–6456. doi:10.1021/acs.chemmater.7b01991.

[6] C.R. Ryder, J. Zhu, J.-H. Lee, S.A. Wells, J.D. Wood, M.C. Hersam, C.A. Husko, J.R. Guest, X. Liu, J. Kang, Stable aqueous dispersions of optically and electronically active phosphorene, Proc. Natl. Acad. Sci. 113 (2016) 11688–11693. doi:10.1073/pnas.1602215113.

[7] A. Dettlaff, G. Skowierzak, Ł. Macewicz, M. Sobaszek, J. Karczewski, M. Sawczak, J. Ryl, T. Ossowski, R. Bogdanowicz, Electrochemical Stability of Few-Layered Phosphorene Flakes on Boron-Doped Diamond: A Wide Potential Range of Studies in Aqueous Solutions, J. Phys. Chem. C. 123 (2019) 20233–20240.

doi:10.1021/acs.jpcc.9b03028.

[8] M. Hermes, F. Scholz, The electrochemical oxidation of white phosphorus at a three-phase junction, Electrochem. Commun. 2 (2000) 845–850. doi:10.1016/S1388-2481(00)00134-X.

[9] L. Wang, Z. Sofer, M. Pumera, Voltammetry of Layered Black Phosphorus: Electrochemistry of Multilayer Phosphorene, ChemElectroChem. 2 (2015) 324–327. doi:10.1002/celc.201402363.

[10] Q. Li, J.T. Wu, Y. Liu, X.M. Qi, H.G. Jin, C. Yang, J. Liu, G.L. Li, Q.G. He, Recent advances in black phosphorus-based electrochemical sensors: A review, Anal. Chim. Acta. 1170 (2021) 338480. doi:10.1016/j.aca.2021.338480.

[11] L. Shao, H. Sun, L. Miao, X. Chen, M. Han, J. Sun, S. Liu, L. Li, F. Cheng, J. Chen, Facile preparation of NH2-functionalized black phosphorene for the electrocatalytic hydrogen evolution reaction, J. Mater. Chem. A. 6 (2018) 2494–2499. doi:10.1039/c7ta10884b.

[12] P.K. Sarswat, M.L. Free, Real-Time Detection of Thiols Using CoPc Modified Black-Phosphorus Based Sensors, J. Electrochem. Soc. 166 (2019) B1–B8. doi:10.1149/2.0111905jes.

[13] L. Durai, A. Gopalakrishnan, N. Vishnu, S. Badhulika, Polyaniline Sheathed Black Phosphorous: A Novel, Advanced Platform for Electrochemical Sensing Applications, Electroanalysis. 32 (2020) 238–247. doi:10.1002/elan.201900483.

[14] X. Niu, W. Weng, C. Yin, Y. Niu, G. Li, R. Dong, Y. Men, W. Sun, R. Dong, G. Li, C. Yin, X. Niu, W. Weng, W. Sun, Black phosphorene modified glassy carbon electrode for the sensitive voltammetric detection of rutin, J. Electroanal. Chem. 811 (2018) 78–83. doi:10.1016/j.jelechem.2018.01.038.

[15] J.E.S. Fonsaca, S.H. Domingues, E.S. Orth, A.J.G. Zarbin, Air stable black phosphorous in polyaniline-based nanocomposite, Sci. Rep. 7 (2017) 1–9. doi:10.1038/s41598-017-10533-5.

[16] T.P. Wang, C.L. Lee, C.H. Kuo, W.C. Kuo, Promising activities of defective black phosphorus nanosheets as non-enzymatic hydrogen peroxide sensors, Appl. Surf. Sci. 542 (2021) 148588. doi:10.1016/j.apsusc.2020.148588.

[17] Z. Zhang, Y. Li, J. Xu, Y. Wen, Electropolymerized molecularly imprinted polypyrrole decorated with black phosphorene quantum dots onto poly(3,4-ethylenedioxythiophene) nanorods and its voltammetric sensing of vitamin C, J. Electroanal. Chem. 814 (2018) 153–160. doi:10.1016/j.jelechem.2018.02.059.

[18] Y. Zhao, Y.-H. Zhang, Z. Zhuge, Y.-H. Tang, J.-W. Tao, Y. Chen, Synthesis of a Poly-L-lysine/Black Phosphorus Hybrid for Biosensors, Anal. Chem. (2018) acs.analchem.7b04395. doi:10.1021/acs.analchem.7b04395.

[19] L. Wu, Q. Meng, Z. Xu, Q. Cao, Y. Xiao, H. Liu, G. Han, S. Wei, Passivation of black phosphorus as organic-phase enzyme platform for bisphenol A determination, Anal. Chim. Acta. 1095 (2020) 197–203. doi:10.1016/j.aca.2019.10.030.

[20] F. Li, Z. Yu, X. Han, R.Y. Lai, Electrochemical aptamer-based sensors for food and water analysis: A review, Anal. Chim. Acta. 1051 (2019) 1–23. doi:10.1016/j.aca.2018.10.058.

[21] P. Jakóbczyk, M. Kowalski, M. Brodowski, A. Dettlaff, B. Dec, D. Nidzworski, J. Ryl, T. Ossowski, R. Bogdanowicz, Low-power microwave-induced fabrication of functionalised few-layer black phosphorus electrodes : A novel route towards Haemophilus Influenzae pathogen biosensing devices, Appl. Surf. Sci. 539 (2021) 148286. doi:10.1016/j.apsusc.2020.148286.

[22] C.C. Mayorga-Martinez, N. Mohamad Latiff, A.Y.S. Eng, Z. Sofer, M. Pumera, Black Phosphorus Nanoparticle Labels for Immunoassays via Hydrogen Evolution Reaction Mediation, Anal. Chem. 88 (2016) 10074–10079. doi:10.1021/acs.analchem.6b02422.

[23] S. Liu, J. Luo, X. Jiang, X. Li, M. Yang, Gold nanoparticle–modified black phosphorus nanosheets with improved stability for detection of circulating tumor cells, Microchim. Acta. 187 (2020). doi:10.1007/s00604-020-04367-8.

[24] L. Zhang, K.J. Tian, Y.P. Dong, H.C. Ding, C.M. Wang, Electrogenerated chemiluminescence of Ru(bpy)32+ at a black phosphorus quantum dot modified electrode and its sensing application, Analyst. 143 (2018) 304–310. doi:10.1039/c7an01617d.

[25] H. Liu, Y. Zhang, Y.P. Dong, X.F. Chu, Electrogenerated chemiluminescence aptasensor for lysozyme based on copolymer nanospheres encapsulated black phosphorus quantum dots, Talanta. 199 (2019) 507–512. doi:10.1016/j.talanta.2019.02.099.

[26] J. Plutnar, Z. Sofer, M. Pumera, Products of degradation of black phosphorus in protic solvents, ACS Nano. 12 (2018) 8390–8396. doi:10.1021/acsnano.8b03740.

[27] Q. Zhou, Q. Chen, Y. Tong, J. Wang, Light-Induced Ambient Degradation of Few-Layer Black Phosphorus: Mechanism and Protection, Angew. Chemie - Int. Ed. 55 (2016) 11437–11441. doi:10.1002/anie.201605168.

[28] Y. Huang, J. Qiao, K. He, S. Bliznakov, E. Sutter, X. Chen, D. Luo, F. Meng, D. Su, J. Decker, W. Ji, R.S. Ruoff, P. Sutter, Interaction of black phosphorus with oxygen and water, Chem. Mater. 28 (2016) 8330–8339. doi:10.1021/acs.chemmater.6b03592.

[29] L. Zhang, L.F. Gao, L. Li, C.X. Hu, Q.Q. Yang, Z.Y. Zhu, R. Peng, Q. Wang, Y. Peng, J. Jin, H.L. Zhang, Negatively charged 2D black phosphorus for highly efficient covalent functionalization, Mater. Chem. Front. 2 (2018) 1700–1706. doi:10.1039/c8qm00237a.

[30] Y. Liu, P. Gao, T. Zhang, X. Zhu, M. Zhang, M. Chen, P. Du, G.W. Wang, H. Ji, J. Yang, S. Yang, Azide Passivation of Black Phosphorus Nanosheets: Covalent Functionalization Affords Ambient Stability Enhancement, Angew. Chemie - Int. Ed. 58 (2019) 1479–1483. doi:10.1002/anie.201813218.

[31] Z. Sofer, J. Luxa, D. Bouša, D. Sedmidubský, P. Lazar, T. Hartman, H. Hardtdegen, M. Pumera, The Covalent Functionalization of Layered Black Phosphorus by Nucleophilic Reagents, Angew. Chemie - Int. Ed. 56 (2017) 9891–9896. doi:10.1002/anie.201705722.

[32] R. Gusmão, Z. Sofer, M. Pumera, Functional Protection of Exfoliated Black Phosphorus by Noncovalent Modification with Anthraquinone, ACS Nano. 12 (2018) 5666–5673. doi:10.1021/acsnano.8b01474.

[33] M. Biedulska, P. Jakóbczyk, M. Sosnowska, B. Dec, A. Muchlińska, A.J. Zaczek, D.

Nidzworski, R. Bogdanowicz, Cytocompatibility of stabilized black phosphorus nanosheets tailored by directly conjugated polymeric micelles for human breast cancer therapy, Sci. Rep. 11 (2021) 1–17. doi:10.1038/s41598-021-88791-7.

[34] Y. Kong, X. Shan, J. Ma, M. Chen, Z. Chen, A novel voltammetric sensor for ascorbic acid based on molecularly imprinted poly(o-phenylenediamine-co-o-aminophenol), Anal. Chim. Acta. 809 (2014) 54–60. doi:10.1016/j.aca.2013.12.003.

[35] Y.L. Suw, I.C. Jung, S.J. Young, W.J. Woon, J.L. Hye, H.L. Seong, Electrochemical detection of ascorbic acid (vitamin C) using a glassy carbon electrode, Nahrung - Food. 48 (2004) 201–204. doi:10.1002/food.200300394.

[36] L. Özcan, M. Şahin, Y. Şahin, Electrochemical preparation of a molecularly imprinted polypyrrole-modified pencil graphite electrode for determination of ascorbic acid, Sensors. 8 (2008) 5792–5805. doi:10.3390/s8095792.

[37] A.E.D. Lalaouna, Y. Hadef, A. Nekkaa, F. Titel, F. Dalia, Cost-effective and earth-friendly chemometrics-assisted spectrophotometric methods for simultaneous determination of Acetaminophen and Ascorbic Acid in pharmaceutical formulation, Spectrochim. Acta - Part A Mol. Biomol. Spectrosc. 266 (2022) 120422. doi:10.1016/j.saa.2021.120422.

[38] S.F. El-Malla, R.H. Elattar, A.H. Kamal, F.R. Mansour, A highly sensitive switch-on spectrofluorometric method for determination of ascorbic acid using a selective eco-friendly approach, Spectrochim. Acta - Part A Mol. Biomol. Spectrosc. 270 (2022) 120802. doi:10.1016/j.saa.2021.120802.

[39] Y.N. Wang, S.D. Wang, Y. Fan, L. Yu, R.H. Zha, L.J. Liu, L.M. Wen, X.P. Chang, H.Q. Liu, G.D. Zou, A dual-chemosensor based on Ni-CP: Fluorescence turn-on sensing toward ascorbic acid and turn-off sensing toward acetylacetone, J. Lumin. 243 (2022). doi:10.1016/j.jlumin.2021.118680.

[40] U. Alvarado, A. Zamora, O. Arango, J. Saldo, M. Castillo, Prediction of riboflavin and ascorbic acid concentrations in skimmed heat-treated milk using front-face fluorescence spectroscopy, J. Food Eng. 318 (2022) 110869. doi:10.1016/j.jfoodeng.2021.110869.

[41] I. Dioha, O. Olugbemi, T. Onuegbu, Z. Shahru, Determination of ascorbic acid content of some tropical fruits by iodometric titration, Int. J. Biol. Chem. Sci. 5 (2012) 2180. doi:10.4314/ijbcs.v5i5.37.

[42] A.P.S. Paim, C.M.N.V. Almeida, B.F. Reis, R.A.S. Lapa, E.A.G. Zagatto, J.L.F. Costa Lima, Automatic potentiometric flow titration procedure for ascorbic acid determination in pharmaceutical formulations, J. Pharm. Biomed. Anal. 28 (2002) 1221–1225. doi:10.1016/S0731-7085(02)00018-3.

[43] L.A. Tortajada-Genaro, Determination of L-Ascorbic Acid in Tomato by Capillary Electrophoresis, J. Chem. Educ. 89 (2012) 1194–1197. doi:10.1021/ed200875a.

[44] L. Nováková, P. Solich, D. Solichová, HPLC methods for simultaneous determination of ascorbic and dehydroascorbic acids, TrAC - Trends Anal. Chem. 27 (2008) 942–958. doi:10.1016/j.trac.2008.08.006.

[45] Z. Gazdik, O. Zitka, J. Petrlova, V. Adam, J. Zehnalek, A. Horna, V. Reznicek, M. Beklova, R. Kizek, Determination of Vitamin C (Ascorbic Acid) Using High

Performance Liquid Chromatography Coupled with Electrochemical Detection, Sensors. 8 (2008) 7097–7112. doi:10.3390/s8117097.

[46] S.M. Siddeeg, N.S. Alsaiari, M.A. Tahoon, F. Ben Rebah, The application of nanomaterials as electrode modifiers for the electrochemical detection of ascorbic acid: Review, Int. J. Electrochem. Sci. 15 (2020) 3327–3346. doi:10.20964/2020.04.13.

[47] A. Lorenzoni, M. Baldoni, E. Besley, F. Mercuri, Noncovalent passivation of supported phosphorene for device applications: From morphology to electronic properties, Phys. Chem. Chem. Phys. 22 (2020) 12482–12488. doi:10.1039/d0cp00939c.

[48] H. Lee, S. Lim, Thermophysical Properties of Microelectronic Substrates Finished with Organic Solderability Preservatives, Electron. Mater. Lett. 3 (2007) 177–183. http://www.papersearch.net/view/detail.asp?detail_key=04218644.

[49] M.C. Granger, G.M. Swain, The Influence of Surface Interactions on the Reversibility of Ferri/Ferrocyanide at Boron-Doped Diamond Thin-Film Electrodes, J. Electrochem. Soc. 146 (1999) 4551–4558. doi:10.1149/1.1392673.

[50] P. Chen, R.L. McCreery, Control of Electron Transfer Kinetics at Glassy Carbon Electrodes by Specific Surface Modification, Anal. Chem. 68 (1996) 3958–3965. doi:10.1021/ac960492r.

[51] J. V. Macpherson, A practical guide to using boron doped diamond in electrochemical research, Phys. Chem. Chem. Phys. 17 (2015) 2935–2949. doi:10.1039/c4cp04022h.

[52] R.S. Nicholson, Theory and Application of Cyclic Voltammetry for Measurement of Electrode Reaction Kinetics, Anal. Chem. 37 (1965) 1351–1355. doi:10.1021/ac60230a016.

[53] M. Pierpaoli, A. Dettlaff, M. Szopińska, K. Karpienko, M. Wróbel, A. Łuczkiewicz, S. Fudala-Książek, R. Bogdanowicz, Simultaneous opto-electrochemical monitoring of carbamazepine and its electro-oxidation by-products in wastewater, J. Hazard. Mater. 419 (2021). doi:10.1016/j.jhazmat.2021.126509.

[54] L.R.F. A.J. Bard, Electrochemical Methods. Fundamentals and Applications., second, John Wiley & Sons, Ltd, 2001.

[55] A. Dettlaff, M. Sobaszek, T. Klimczuk, R. Bogdanowicz, Enhanced electrochemical kinetics of highly-oriented (111)-textured boron-doped diamond electrodes induced by deuterium plasma chemistry, Carbon N. Y. 174 (2021) 594–604. doi:10.1016/j.carbon.2020.11.096.

[56] C.E.B. R.G. Compton, Understanding Voltammetry, Word Scientific, 2018.

[57] C.G. Zoski, ed., Handbook of Electrochemistry, Elsevier Science, 2007.

[58] N. Wendy Maxakato, S. Surprise Gwebu, G. Hlengiwe Mhlongo, eds., Voltammetry, IntechOpen, 2019. doi:10.5772/intechopen.75223.

[59] G. Wilson, Electrochemistry: Principles, Methods, and Applications, Bioelectrochemistry Bioenerg. 34 (1994) 207. doi:10.1016/0302-4598(94)80039-1.

[60] V.C. Diculescu, S. Kumbhat, A.M. Oliveira-Brett, Electrochemical behaviour of isatin at a glassy carbon electrode, Anal. Chim. Acta. 575 (2006) 190–197. doi:10.1016/j.aca.2006.05.091.

[61] W. Kit-Anan, A. Olarnwanich, C. Sriprachuabwong, C. Karuwan, A. Tuantranont, A. Wisitsoraat, W. Srituravanich, A. Pimpin, Disposable paper-based electrochemical sensor utilizing inkjet-printed Polyaniline modified screen-printed carbon electrode for Ascorbic acid detection, J. Electroanal. Chem. 685 (2012) 72–78. doi:10.1016/j.jelechem.2012.08.039.

[62] P. Kannan, S.A. John, Determination of nanomolar uric and ascorbic acids using enlarged gold nanoparticles modified electrode, Anal. Biochem. 386 (2009) 65–72. doi:10.1016/j.ab.2008.11.043.